FERMILAB-CONF-75-141-E #87A

Presented at the International Symposium on Lepton and Photon Interactions, Stanford, August (1975).

Photoproduction of New Particle at Fermilab *

Wonyong Lee

Columbia University, New York, N.Y. 10027

I was asked to talk about high energy photon experiments at Fermilab.

There are two high energy photon beams at Fermi National Accelerator Laboratory. The first one to come into operation was the wide band photon beam. A group of physicists from Columbia, Cornell, Hawaii, Illinois and Fermilab observed ψ/J production[1] in reactions induced by photons and neutrons from this beam.[2] This morning T. O'Halloran discussed the neutron experiment. I will concentrate on the recent results in the photoproduction experiment conducted in this same beam. The other photon beam is a high energy electron/tagged photon beam. Let me first talk about this beam.

Tagged Photon Beam

Over the past year, a high energy electron/tagged photon beam has been installed and brought into operation in the Proton East Area at Fermilab. The full facility has been used since the end of June for high energy photoproduction experiments by a group from Fermilab, Lebedev, Santa Barbara, and Toronto. Figure 1 shows schematically the layout of the facility. A Be target is used to produce a neutral beam. Photons are converted to electrons in a lead radiator. The electrons are transported over 300 m to the tagging system where they hit a radiator, produce a bremsstrahlung beam, and are bent into 12 lead glass counters. In the lead glass counter hodoscope, the electron energy is measured to tag the photons.

The electron beam has been tuned from 40 GeV to 225 GeV with 300 GeV protons incident on the Be target and is now running at 90 GeV with a 400 GeV proton beam. Preliminary measurements of the photon flux are consistent with the calculated

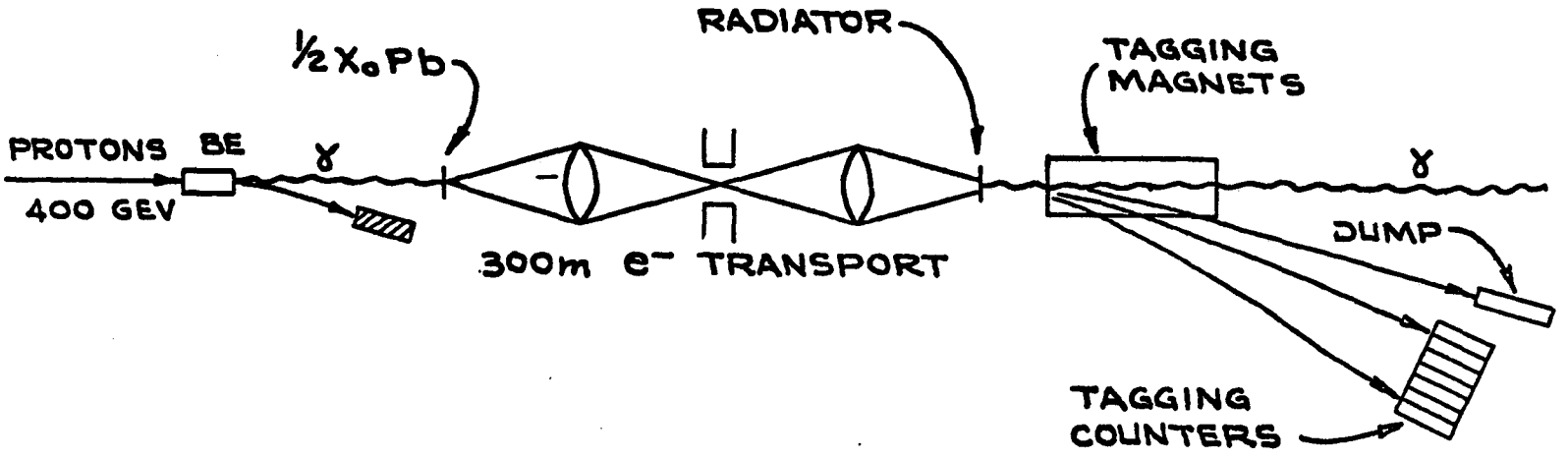

Fig. 1 Layout of the electron/tagged photon beam

flux, shown in Fig. 2, within a factor of two.[3] The pion contamination has been crudely measured to be below 0.4% at 115 GeV. The tagging system has been tuned with 40, 90 and 115 GeV electrons with a 0.2% radiator. The momentum acceptance of the electron beam is $\pm$ 4 1/2% and thus dominates the tagged photon energy resolution. The false tag rate at 115 GeV is $\sim$ 0.3%.

At 115 GeV, the electron beam halo contributes only a small fraction of the false tag rate. The false tag levels of the system are already satisfactory for the most demanding experiment in this regard, the photon total cross section to be measured during the coming year.

The tagging range is approximately 60% of the bremsstrahlung spectrum. In this "clean" mode of operation with a 2.0% radiator, photon fluxes are about 1% of the e^- fluxes. At the present time, the facility is operating in a high intensity mode with a 20% radiator yielding tagged photon fluxes of about 10^6/pulse. The occasional second photon from the thick radiator is detected and subtracted by the experiment. False tags (meaning no photon) are about 1 1/2%.

I would now like to discuss the wide band photon beam experiment.

Wide Band Photon Beam

The photons are obtained from a 0-mr neutral beam which is produced by the interactions of 300/380 GeV protons in a 30.5 cm Be target. The γ-to-n ratio is improved by a factor of roughly 200 above the γ-to-n ratio at production by passing the beam through 34 m of liquid D_2. With the primary proton energy of 300 GeV, the photon spectrum at the experimental target is shown in Fig. 3.

The detector, which is shown in Fig. 4, consists of a multiwire proportional chamber magnetic spectrometer and a particle identifier. The spectrometer magnet M2, which has a field integral of 20 kG m, bends the trajectories of charged particles vertically. The magnet aperture, which is 61 cm high and 40.6 cm wide, determines the acceptance of the spectrometer.

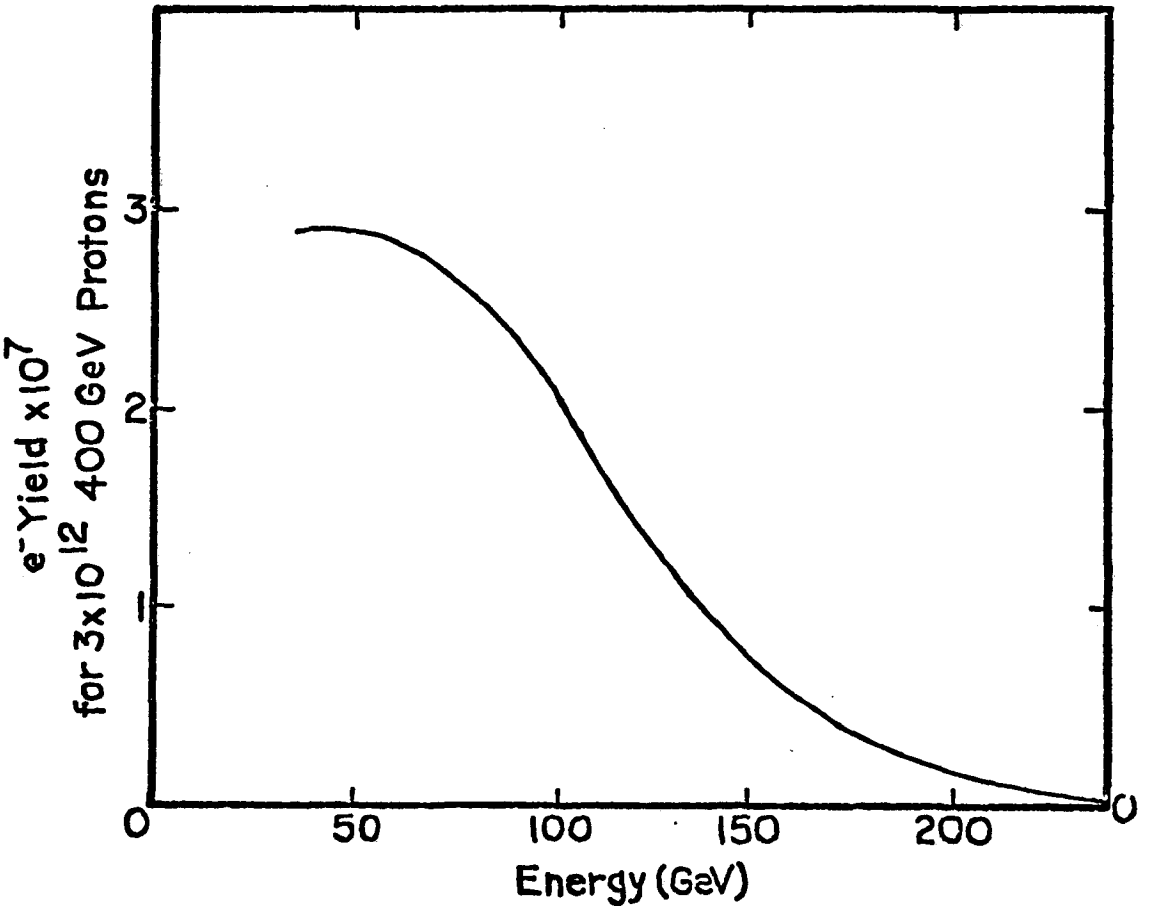

Fig. 2 Electron energy spectrum with 300 GeV proton incident on the Be target

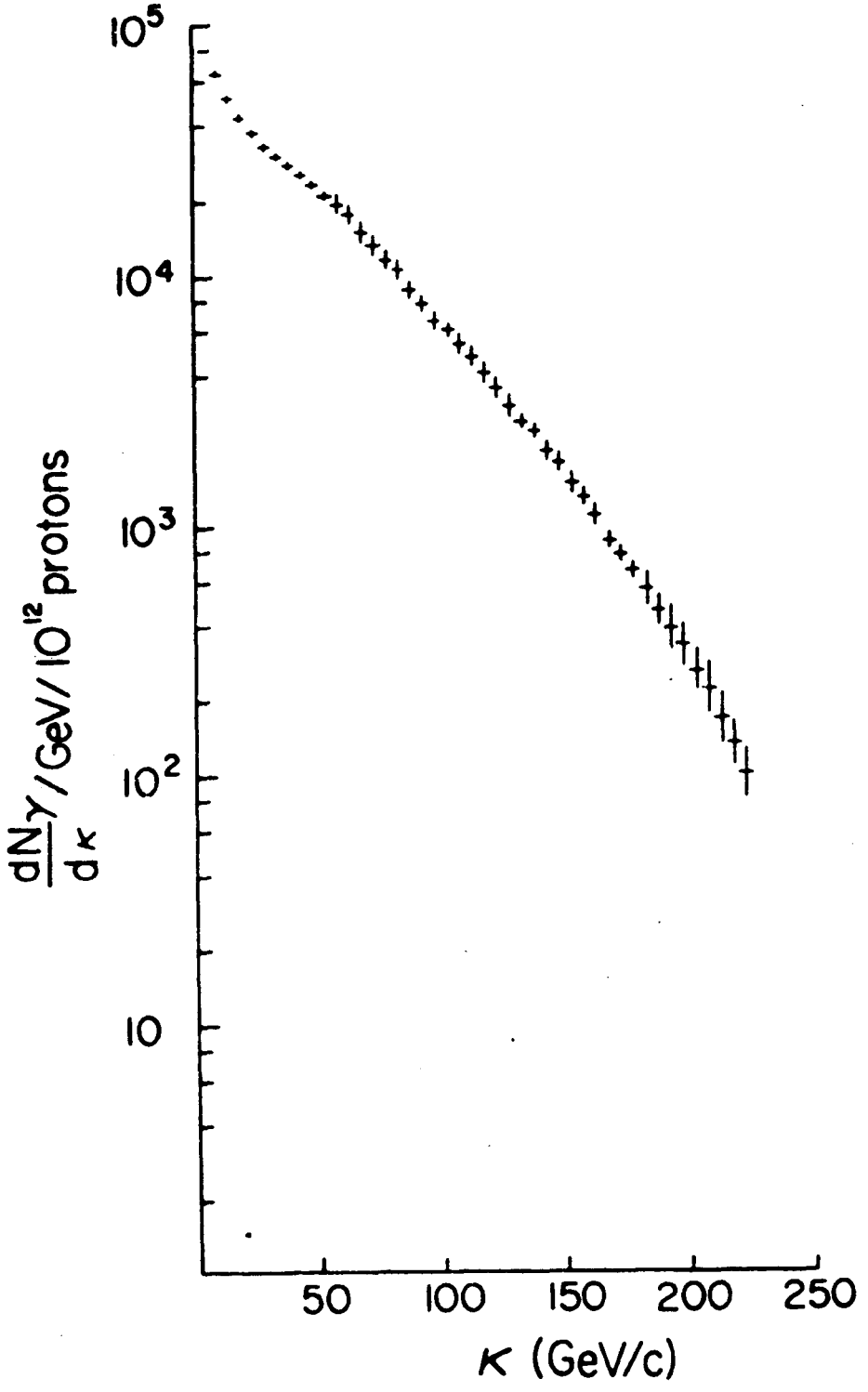

Fig. 3 Photon energy spectrum at photon target with the cryostat filled with liquid D2

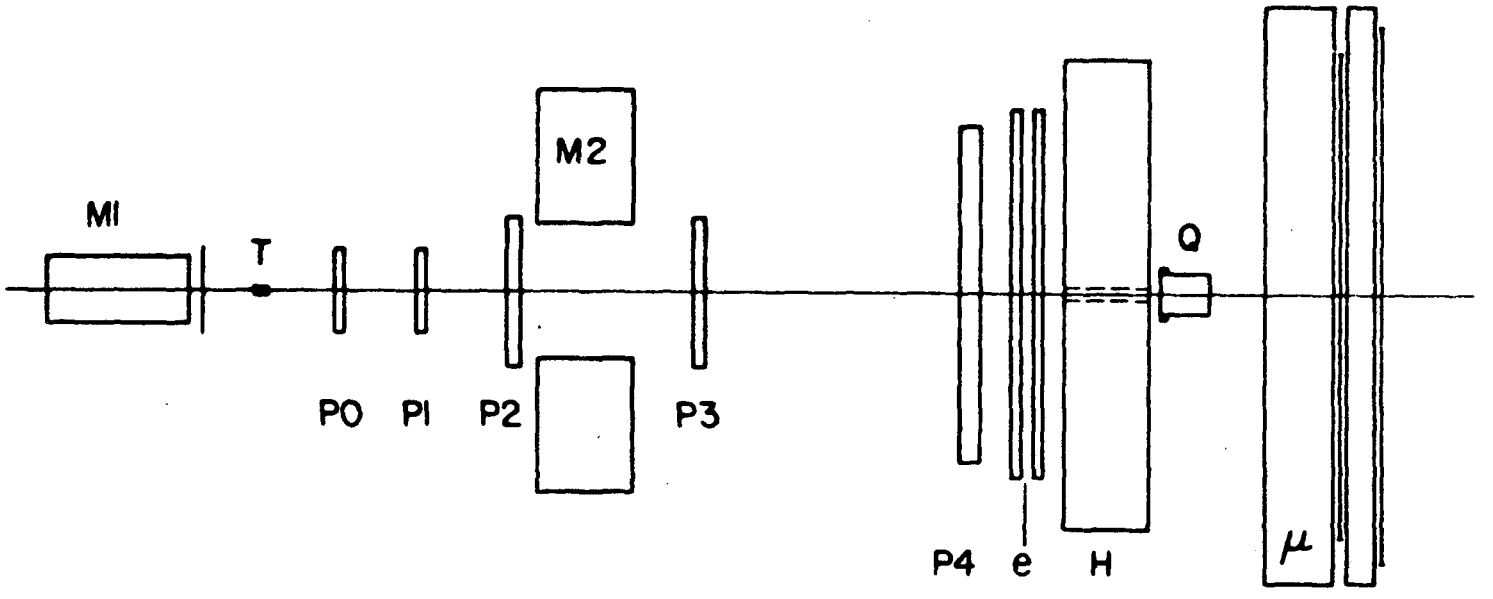

Fig. 4 Layout of detectors in experimental enclosure

Scintillation detectors T, AB and AW, as shown in Fig. 5, cover most of solid angle not covered by multiwire proportional chambers. The counters T are placed to detect recoiling protons and the counters AB and AW covered forward cone.

The particle identifier consists of an electron (and photon) calorimeter, a hadron calorimeter, and a muon identifier, as shown in Fig. 6. The electron calorimeter is made up of an upstream and a downstream shower counter hodoscope. Each hodoscope is split into two identical halves which are separated horizontally from each other by 10 cm, in order to allow the beam and the copiously produced e^+e^- pairs to pass through. Each upstream hodoscope counter contains six layers of lead and plastic, and each counter of the downstream hodoscope contains sixteen layers of lead and plastic. A layer is composed of a 4.8-mm thick plastic scintillator and a 6.3 mm thick Pb sheet.

The hadron calorimeter consists of twenty-four 4.45-cm steel plates interleaved with 6.3-mm sheets of plastic scintillator. A 15-cm square hole allows the beam to pass through the calorimeter. The muon identifier consists of a steel shield which is 60-cm thick, and an 18-element vertical, 22-element horizontal scintillation counter hodoscope.

The photon beam intensity is monitored continuously by a 26-radiation length Wilson quantameter. At regular intervals, the photon spectrum is determined by measuring the total momentum of e^+e^- pairs produced in a 0.04-radiation length lead target. During the calibration runs, the target is inserted in the photon beam in front of a horizontally bending dipole magnet M1 which opens the e^+e^- pairs so that their momentum can be measured in the multiwire proportional chamber spectrometer.

Events which have two or more tracks and which satisfy any of the following requirements are recorded on magnetic tape: Two or more muons in the muon identifier, two or more electrons in the electron calorimeter, one electron and one muon, and, finally, any event which deposits more than a preset amount of energy in the hadron calorimeter.

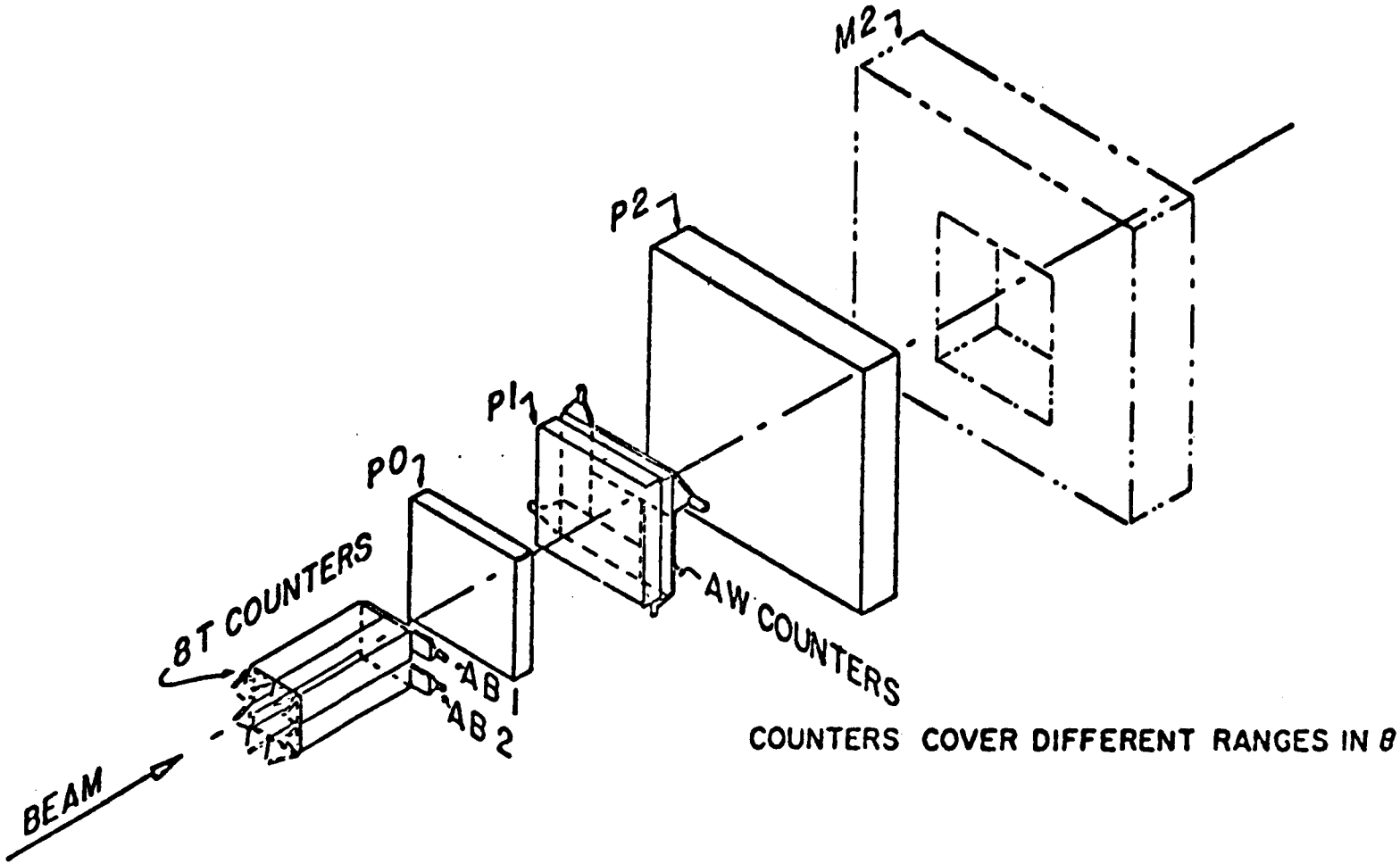

Fig. 5 Layout of scintillation detectors near the photon target

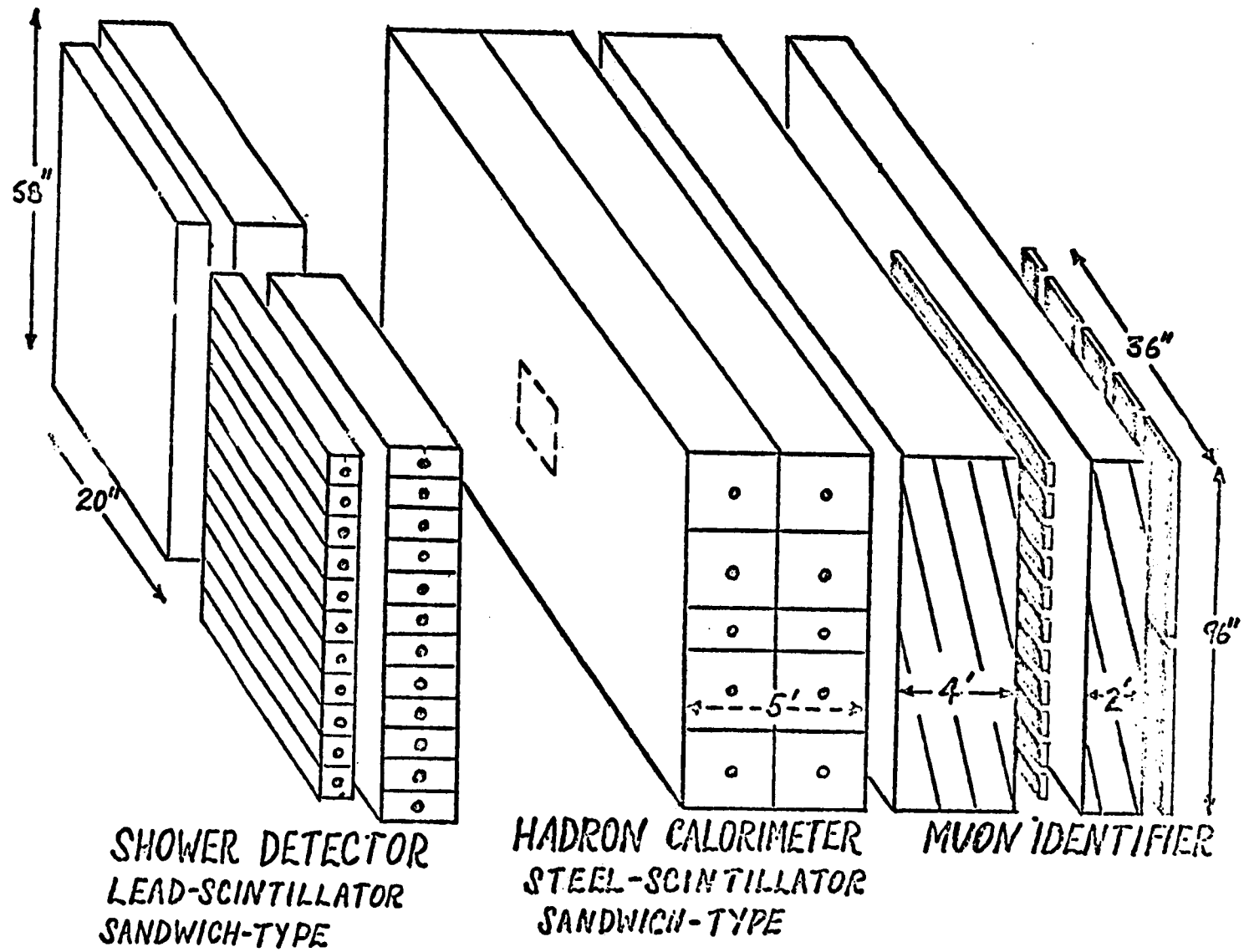

Fig. 6 Layout of particle identifier

For each event, all possible tracks are reconstructed from the multiwire proportional chamber hits.

Let me now discuss the important characteristics of a variety of different final states, beginning with events which possess a dimuon in the final states.

Each track is extrapolated back to each plane of muon counters, and a circle with a radius 2.5 times the expected deviation due to multiple scattering is computed. Any muon counter with a hit which overlaps this circle is considered to be correlated with the track. A "muon" track is required to have correlated hits in both muon counter planes.

The sample of all events with two muon tracks is extracted. The paths of the two muons are extrapolated back to the target to determine if the pair came from a single point within the target. The distance of closest approach, the shortest line segment connecting the two tracks in front of the magnet, is required to be less than 2.5 mm. The vertex of the event is defined to be the midpoint of this line segment. It must be located within 20 cm of the target along the beam direction.

The momentum of each track is computed assuming that the magnetic field is uniform. The momentum resolution in the limit of a uniform field is calculated to be $\delta P/P = \pm 0.03$ (P/100 GeV/c).

The raw mass spectrum for a sample of 60 events with momenta greater than 80 GeV/c is shown in Fig. 7. The two principal features of these data, which can be seen readily, are a preponderance of events at low mass, characteristic of muon-pair production by the Bethe-Heitler mechanism, and a peak at 3.1 GeV/c^2. It should be pointed out that this sample was not restricted to two track events. The width is consistent with our experimental resolution. The data were also taken with the photon target closer to the magnet to obtain events with momenta between 50 GeV and above. The combined data sample, which has 102 events, was used to produce the t distribution shown in Fig. 8. The t distribution for the $\pi^+\pi^-$ final state with a mass of the rho meson has also been studied and shown in Fig. 9. The

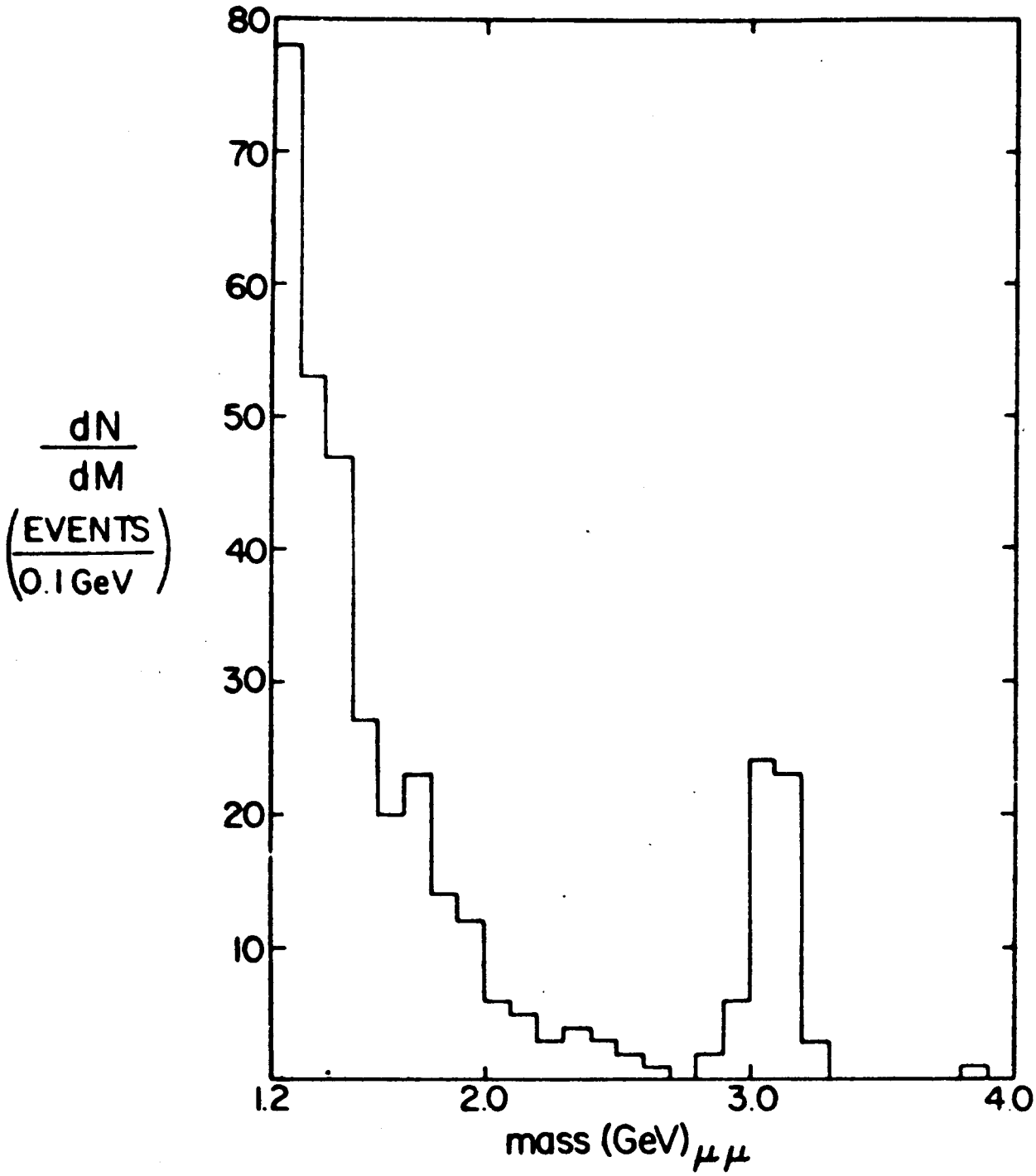

Fig. 7 Dimuon invariant mass distribution observed above 1.2 GeV

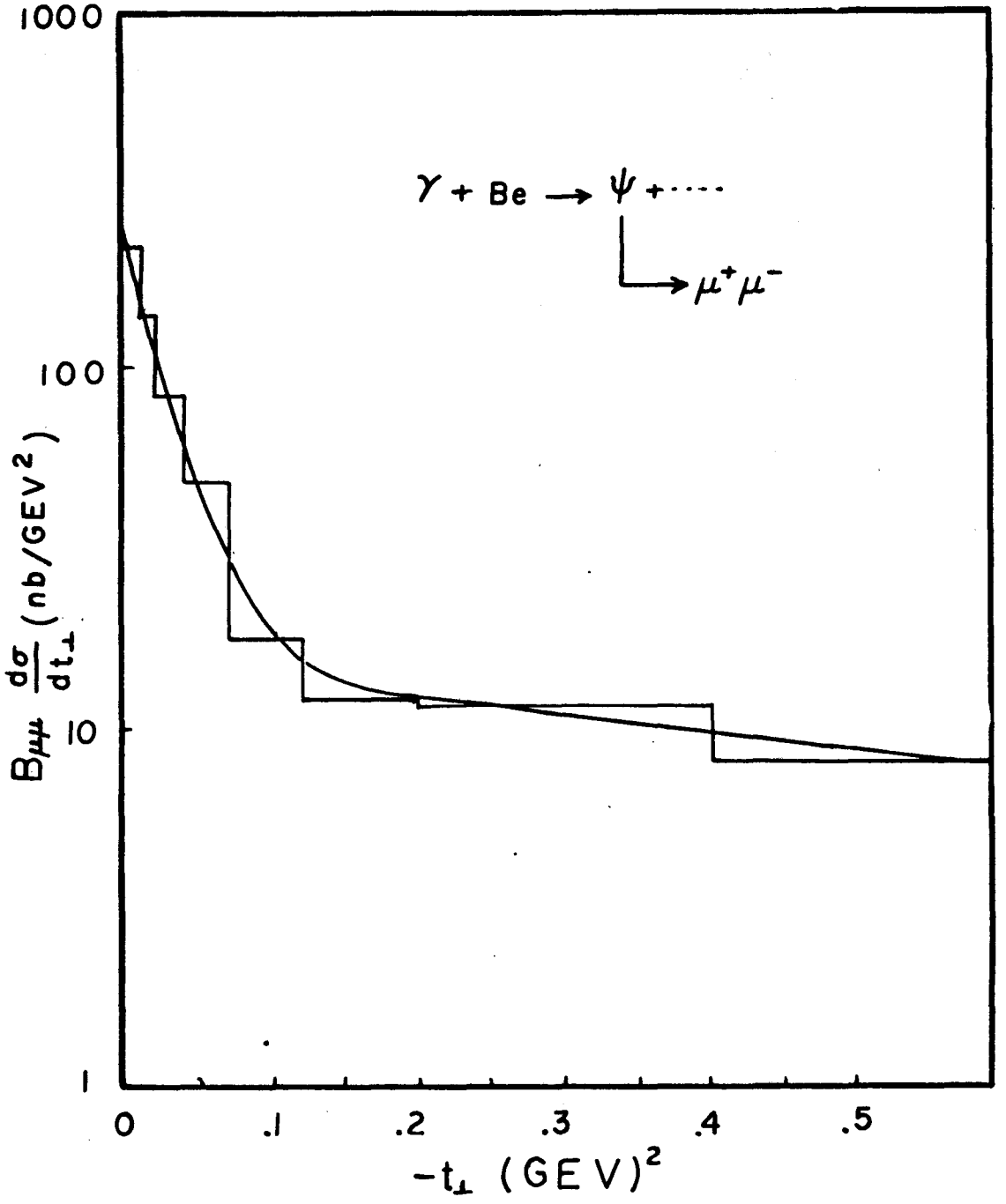

Fig. 8 Observed t distribution for events in 3.1 GeV resonance

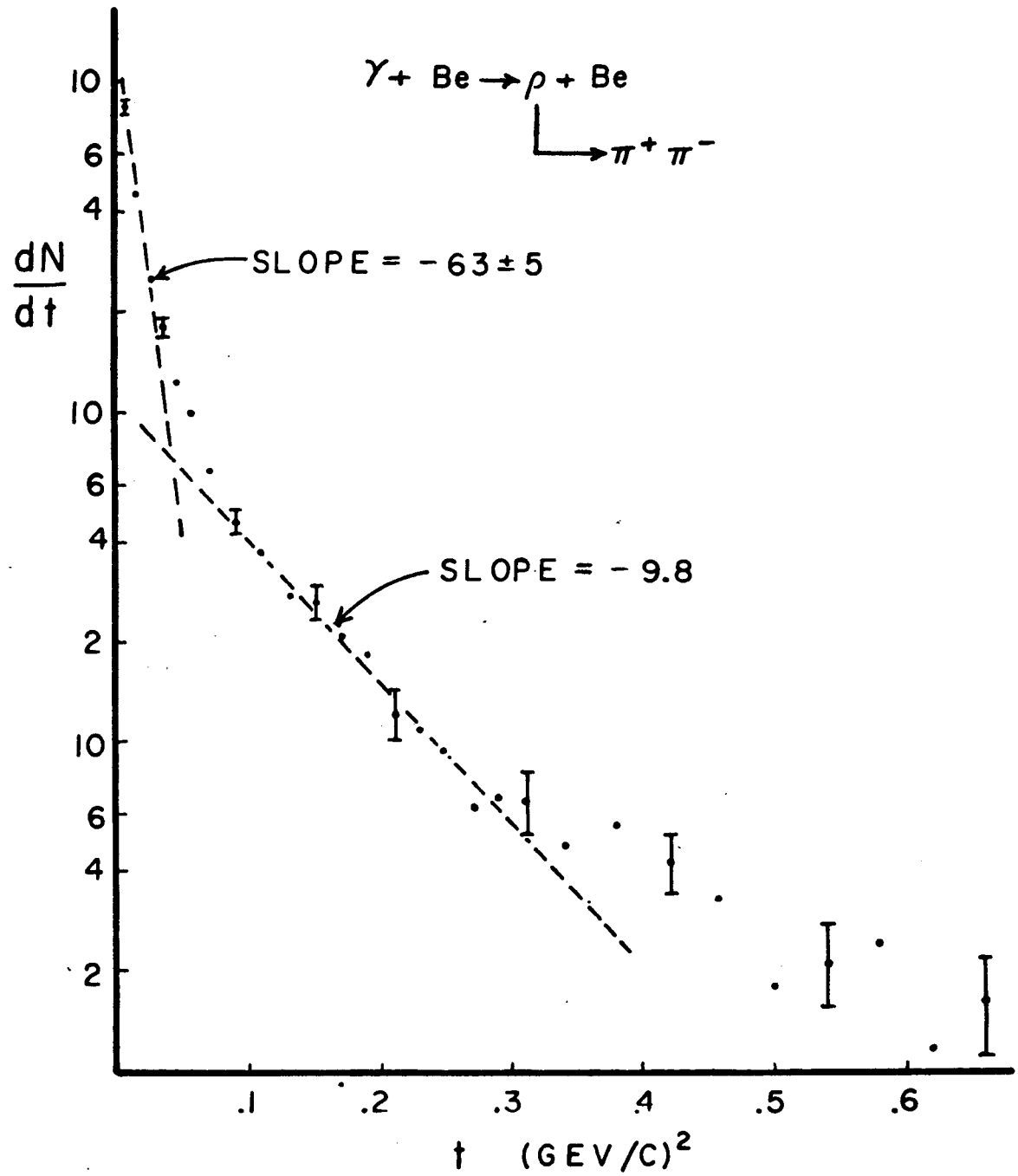

Fig. 9 Observed t distribution for ρ meson

rho data can be fitted very well with the sum of two exponentials, one with a slope of ~ 60 GeV $^{-2}$ which is characteristic of the coherent scattering from the Be nucleus, and the other with a slope of ~ 10 GeV^{-2} which is characteristic of scattering from single nucleons in Be. One can also see these same features in the t distribution of the 3.1 GeV/c^2 resonance. The fitted value of the slope is approximately ~ 50 and ~ 2 GeV $^{-2}$.

There are two principal sources of background in the determination of the ψ cross section.

First we must determine what fraction of the events are produced by hadrons in our beam. Our measured cross section for ψ by neutrons in this beam and the known ratio of photons to neutrons allow us to determine that the number of events in this experiment induced by neutrons is consistent with zero.

The other source of background is the photoproduction of the $\psi'(3700)$ and its decay into $\psi(3100)$ + X with the subsequent decay of the $\psi(3100)$ into two muons.

We have observed two events which are

$$\gamma + \mathrm{Be} \rightarrow \psi'(3700) + \ldots.$$
$$\hookrightarrow \psi(3100) + \pi^+ + \pi^-$$
$$\hookrightarrow \mu^+\mu^- \quad .$$

Based on Monte Carlo calculations, we place an upper limit from this source to be 15% or less.

Based on 102 events and correcting for geometric acceptance and electronic deadtime, we measure:

$$\sigma(\gamma+\mathrm{Be} \rightarrow \psi+\ldots.)\ B(\psi \rightarrow \mu^+\mu^-) = 20 \pm 5 \text{ nb/nucleus} \ .$$

We also determine:

$$\frac{d\sigma}{dt}(\gamma+N \rightarrow \psi+N)\Big|_{t=0} = 55 \pm 24 \text{ nb/GeV}^2 \quad .$$

Here N is a nucleon. This cross section was determined by first determining differential cross section at t = 0 $\frac{d\sigma}{dt}\Big|(\gamma+\mathrm{Be} \rightarrow \psi+\mathrm{Be})\Big|_{t=0}$ and then dividing by A^2, A being the atomic number of Be nucleus.

If we assume the validity of vector dominance and that the forward scattering amplitude is purely imaginary, we obtain for

the ψN total cross section

$\sigma(\psi N) \simeq 1$ mb.

While these assumptions are reasonable for other vector meson photoproduction processes, we have no evidence for their validity in this case.

In order to determine ψN interaction strength without making the above assumptions, we have made a preliminary study of the A dependence of the photoproduction cross section of the ψ. Limiting the ψ events to the small momentum transfer region ($-t < 0.07$ GeV^2), we observed 10 $\psi \to \mu^+\mu^-$ and e^+e^- events in the reaction γ+Pb $\to \psi$+ ... . We would expect to see 11 events if $\sigma(\psi N) = 0$ mb, 5 if $\sigma(\psi N) = 15$ mb, and 4 if $\sigma(\psi N) = 30$ mb. Obviously, we cannot draw any conclusion about the magnitude of $\sigma(\psi N)$ based on our present data. In these calculations, we have used 2.71 fm for the Be radius and 5.66 fm for the Pb nucleus.

Conclusions

1) We observed photoproduction of $\psi(3100)$ and $\psi(3700)$.

2) The $\psi(3100)$ is photoproduced diffractively on the Be nucleus.

3) We find $\sigma(\psi N) \sim 1.0$ mb if we assume vector dominance and that the forward scattering amplitude is purely imaginary.

New Particle Searches

In this section, we will discuss the search for new particles which we have made with our detector. Although we will discuss our search in terms of charmed particles (in a generic sense) and heavy leptons, the objects could be any particles with similar characters.

We do not know the magnitude of the cross section of the reaction γ + Be $\to C^{\bullet} + \bar{C}$ + ..., but we will try to guess. In Table I, we list the total and elastic cross section of vector mesons, ρ, ω, ϕ, and ψ. In calculating these quantities, we make assumptions that vector dominance is valid and the forward scattering amplitude is purely imaginary. For ρ, ω, ϕ, these assumptions are known to be approximately valid. From Table I, we observe that the ratio of elastic to total cross sections is

TABLE I

	Total Cross Section	Elastic Cross Section
$\rho\rho$	25 mb	4 mb
$\omega\rho$	25 mb	4 mb
ϕp	11 mb	1 mb
ψp	1 mb	0.02 mb

10-15% for ρ, ω, ϕ and is only 2% for ψ. Most of the time, there is no ψ in the final state in the interaction of ψ with nucleon. We also know that ψ is not coupled strongly to ordinary hadrons. Therefore, it is possible that most of the time, ψ breaks up into $C + \bar{C}$ when it interacts with nucleon. We can, then, expect the cross section of the reaction $\gamma + Be \rightarrow C\bar{C} + \ldots$ may be as large as $\sim \mu b/Be$. Of course, we have no reason to believe that this estimate is correct.

The reaction $\gamma + Be \rightarrow e^{\pm} + \mu^{\mp} + \nu$'s + ... was used to look for new charged heavy leptons or other pairs of charged particles which then decay into leptons. The procedure is to look for events which contain only a μ and e of opposite charge with no particles other than ν's.

The criteria for the event selection are:

1) There are two and only two tracks and there are no hits in the AB and AW counters near the target.
2) There is no neutral track associated with the event. We require that neither the shower counters nor the hadron calorimeter not associated with the tracks have any measurable energy. For a γ ray, our energy cut is 1.0 GeV.
3) One of the two tracks is a muon using the criteria we have described for ψ photoproduction.

We must now determine if the other track is an electron.

Electron Identification

We define the following terms:

$E_{F(B)}$ = the energy deposited in the front (back) shower counters associated with the track ,

HC = the energy deposited in the hadron calorimeter,

P = the momentum of the track measured by the magnetic spectrometer,

E = $E_F + E_B$.

An electron is identified by two properties:

1) almost all of its energy is contained in the shower counter;
2) it has a characteristic longitudinal shower development.

In Fig. 10, we show E/P for electrons obtained from pair production. The electrons have energies from 7 to 40 GeV.

The data are peaked at 1.0 with a FWHM of ~ 10%.

Electrons can further be identified by their characteristic longitudinal shower development. The variable $f = E_F/E$ and $g = HC/p$ have been studied in the calibration data. With a cut of $g < 0.2$, we lose less than 5% of the electrons. The distribution in f shows a characteristic broad peak centered at 0.4 ~ 0.6 for the energy range of 10-50 GeV. The energy dependence of the value of the peak can be removed by the introduction of $f' = f \frac{\ln(p/22\ \mathrm{MeV})}{3.85}$. Figure 10 shows the distribution of f' for three energy regions. All distributions show a peak at 1.0 with a FWHM ≃ 0.45. A cut of $0.5 < f' < 1.5$ would keep 95% of real electrons of independent electron energy.

The efficiency of these variables in selecting events with an electron can be demonstrated by selecting events with two tracks which form a vertex along the beam line, but not at the target. One of the tracks is consistent with being a hadron which we call a pion. The other track satisfies the cut $E/p > 0.3$. The mass of the two tracks indicates that these are predominantly K^o_{e3} decays. In Fig. 11, we show the E/p and f' distributions for these events. We clearly observe an electron signal and we believe that they are K_{e3}.

For new particle searches, we consider events, which have a clearly identified muon and another track which satisfies the cut $E/p > 0.3$. For these events, we consider the possibility that the electron is a pion which deposited a fraction of its energy in the shower counter and the muon is the product of a pion decay in flight. Considering both of these tracks to be pions after appropriately correcting the muon momentum, we plot the mass distribution of these events, as shown in Fig. 12. We observe a clear ρ^o signal. We make, therefore, a cut on the data sample of $M_{\pi\pi} > 1.1$ GeV.

For our final sample, in addition to the $M_{\pi\pi}$ cut, we impose the cut $0.5 < F' < 1.5$, $G < 0.2$. For these events, we show the

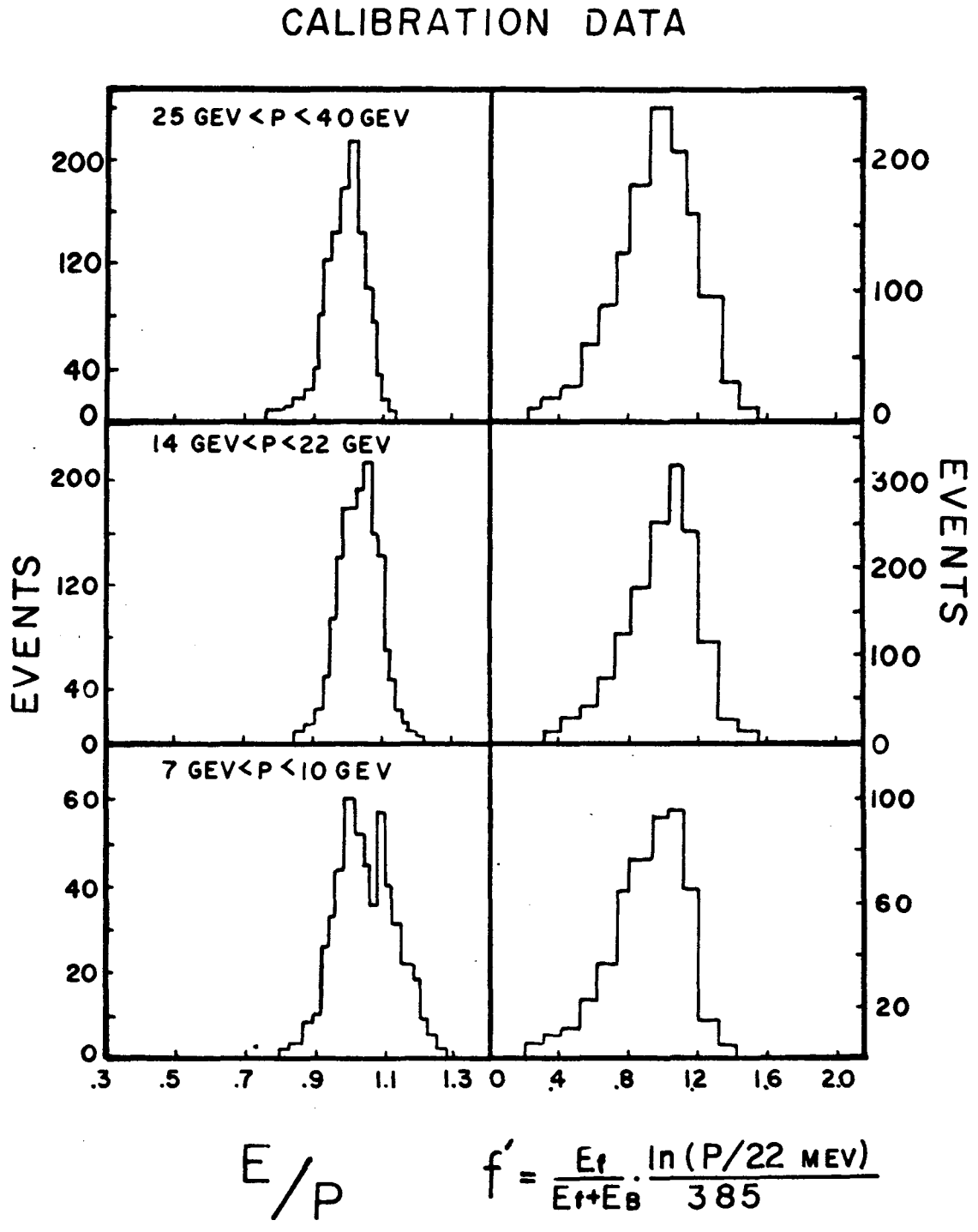

Fig. 10 E/P and f' distribution for three electron energy regions from calibration data

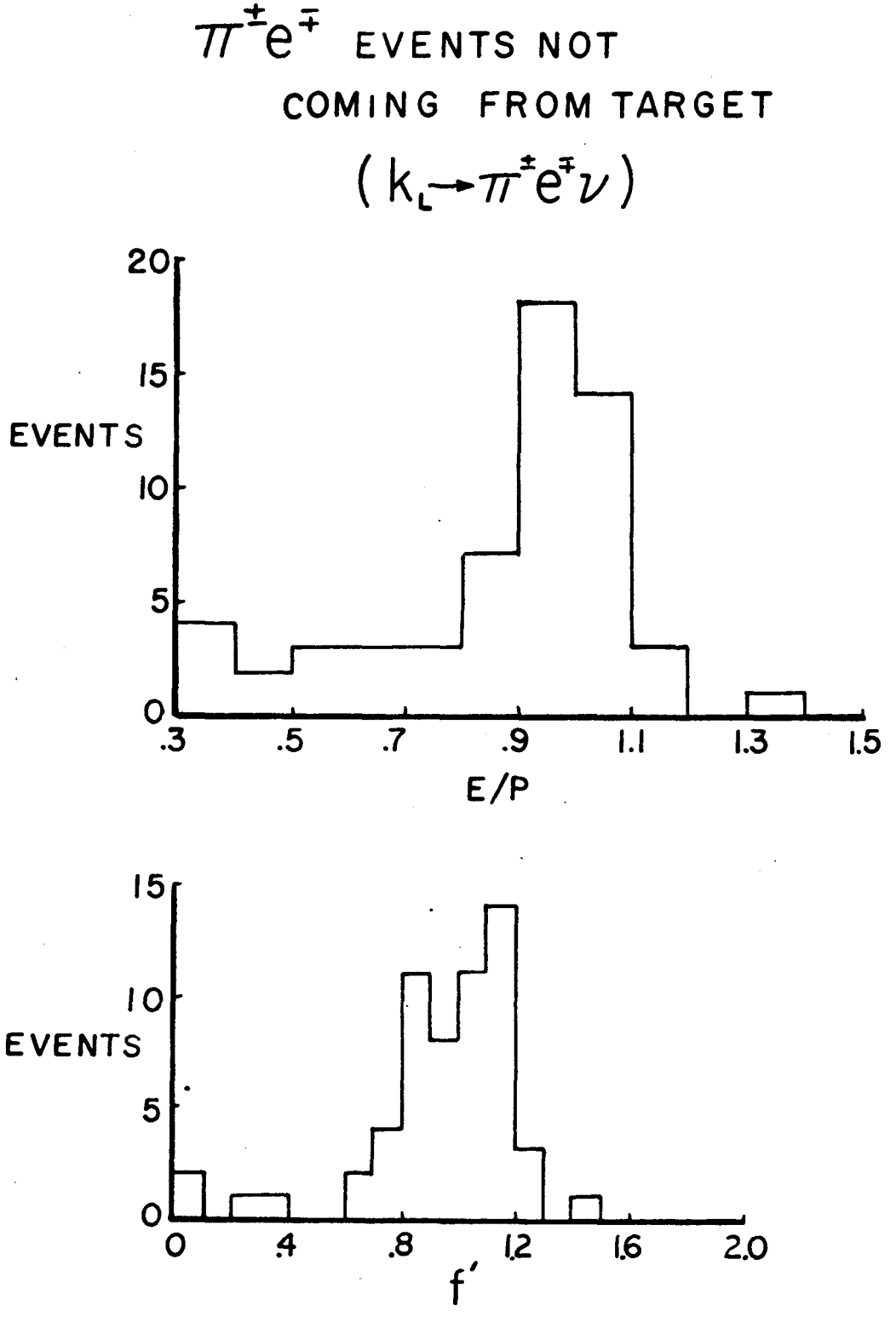

Fig. 11 E/P and f' distribution of electrons from predominantly K_{e3}^{o} decays

distribution of E/p in Fig. 12. Only one event is in the region $0.8 < E/p < 1.2$. We can determine, therefore, that

$$\sigma(\gamma+Be \rightarrow e^{\pm}+\mu^{\mp}+\gamma's \ldots) \times \varepsilon < 6 \times 10^{-34}\ cm^2/Be$$

where the acceptance ε includes:

1) the geometric acceptance of the μ and e in the spectrometer,
2) the mass of the μe pair when interpreted as a $\pi\pi$ pair must be greater than 1.1 GeV.

This limit can be compared to a calculation by P. Tsai.[4]

$$\sigma(\gamma+Be \rightarrow L^{+}L^{-}+ \ldots) = 3.3 \times 10^{-34}\ cm^2/Be$$

for $M_{L^{\pm}} = 2$ GeV, $E_{\gamma} = 100$ GeV. Here L is a heavy lepton. If the branching ratio into a purely leptonic mode is $\sim$ 20%, our limit on the cross section calculated by P. Tsai.

We studied the mass distribution of $K_o+n\pi$, $\Lambda+n\pi$, and $\bar{\Lambda}+n\pi$ to look for charmed hadrons, n = 1,2,3,4. The reaction under consideration is

$$\gamma + Be \rightarrow C + \bar{C} + \ldots$$
$$\hookrightarrow K_o + n\pi\ .$$

Here C is a charmed meson

We identify K_o, Λ, and $\bar{\Lambda}$ through its decay into a pair of charged particles downstream of the production target. The decays are selected by requiring 1) two tracks verticize downstream of the target, and 2) the neutral parent particle verticize with the rest of the particles in the reaction at the target. The mass of two tracks are calculated assuming that both of them are pions and the distribution is shown in Fig. 13. We observe a clear peak in the K_o mass. We observe that the background to the signal ratio is < 10% and the FWHM of the K_o mass is 8 MeV. In Figs. 14 and 16, we show the mass distribution of $K_o\pi^{\pm}$ and $K_o\pi^{+}\pi^{-}$ in the photon induced reactions. We see no statistically significant peak above the mass of 1.5 GeV. We should remark here that $\sim$ 50% of the events here are induced by hadrons, mostly K_L^o. In Fig. 15, we show $K_o\pi^{+}\pi^{-}$ mass distribution when we insert Pb in the beam to attenuate photons and enhance the K_L^o component in the

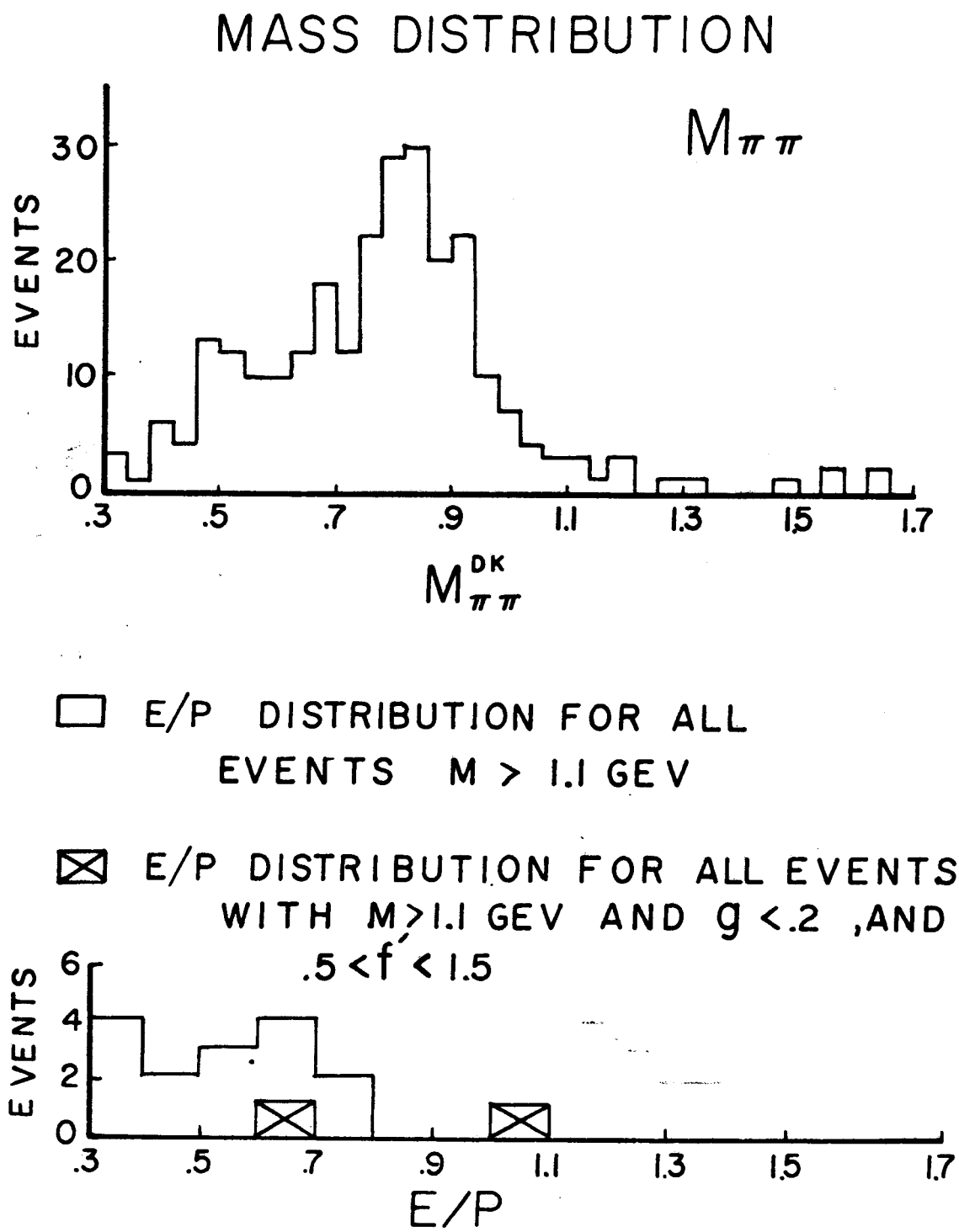

Fig. 12 Mass distribution of μ and electron-like track (E/P > 0.3) and E/P distribution for all events with $M_{\pi\pi}$ > 1.1 GeV, g < 0.2 and 0.5 < f' < 1.5

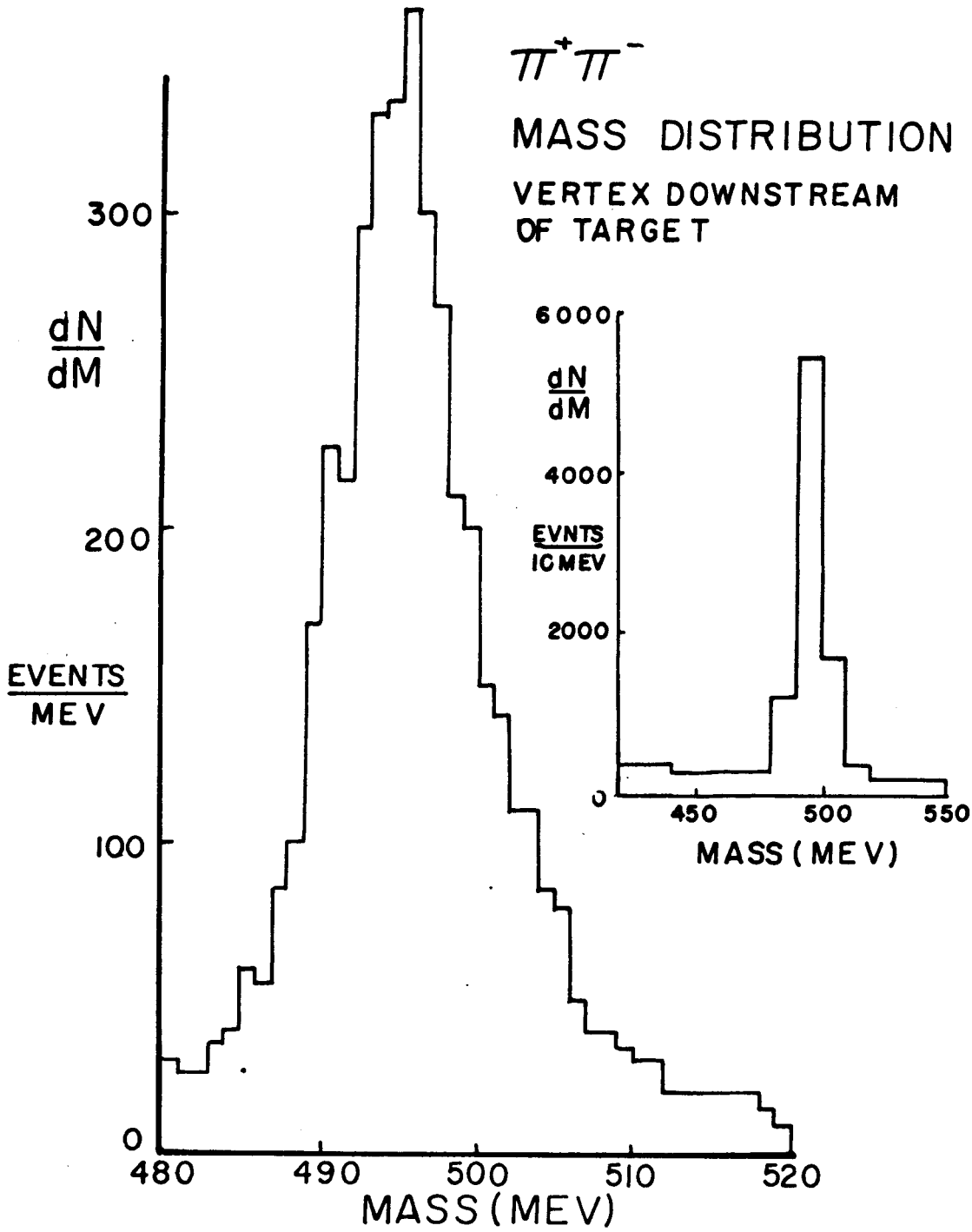

Fig. 13 Mass distribution of V particles

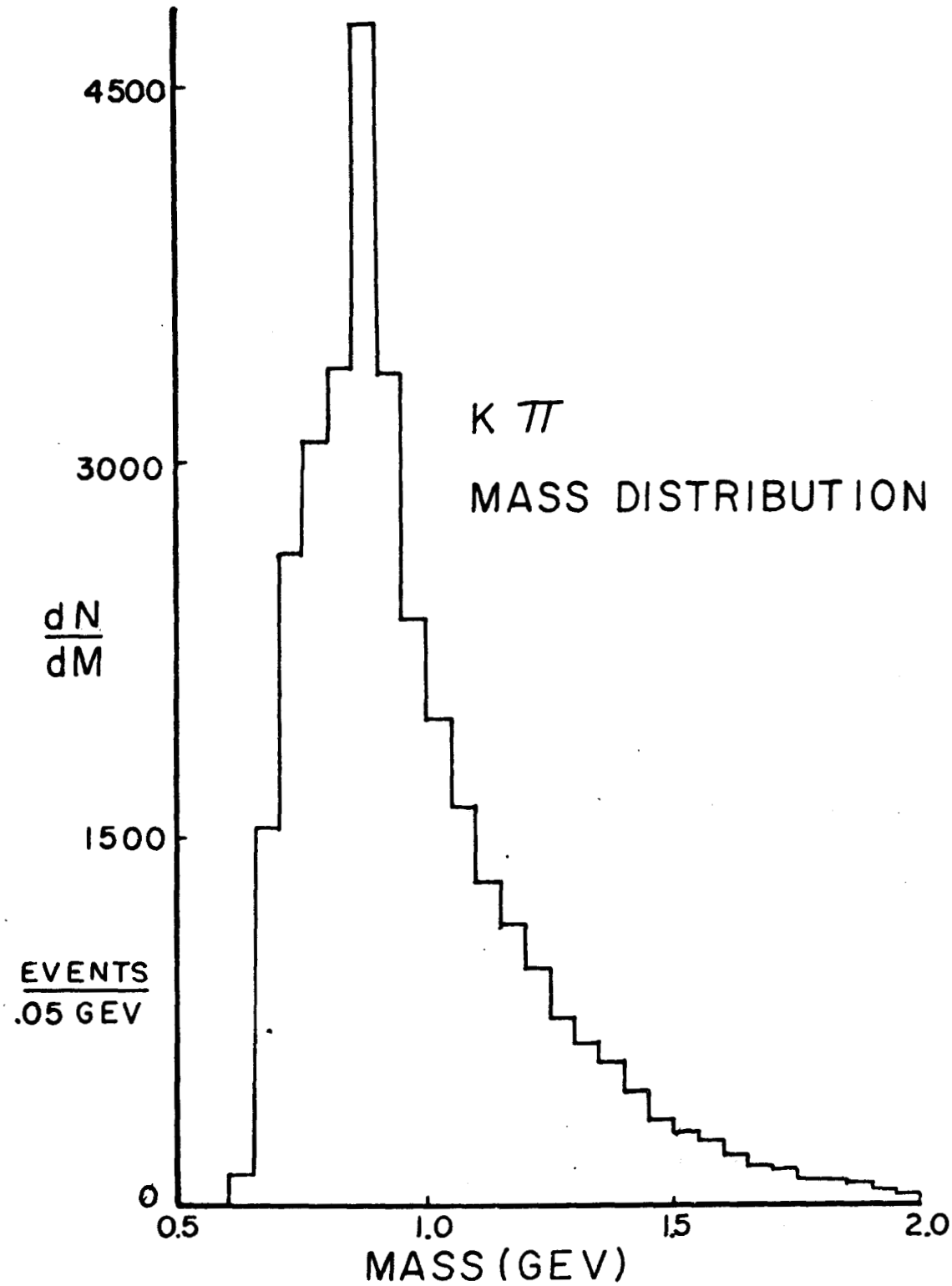

Fig. 14 Mass distribution of $K_o\pi^{\pm}$

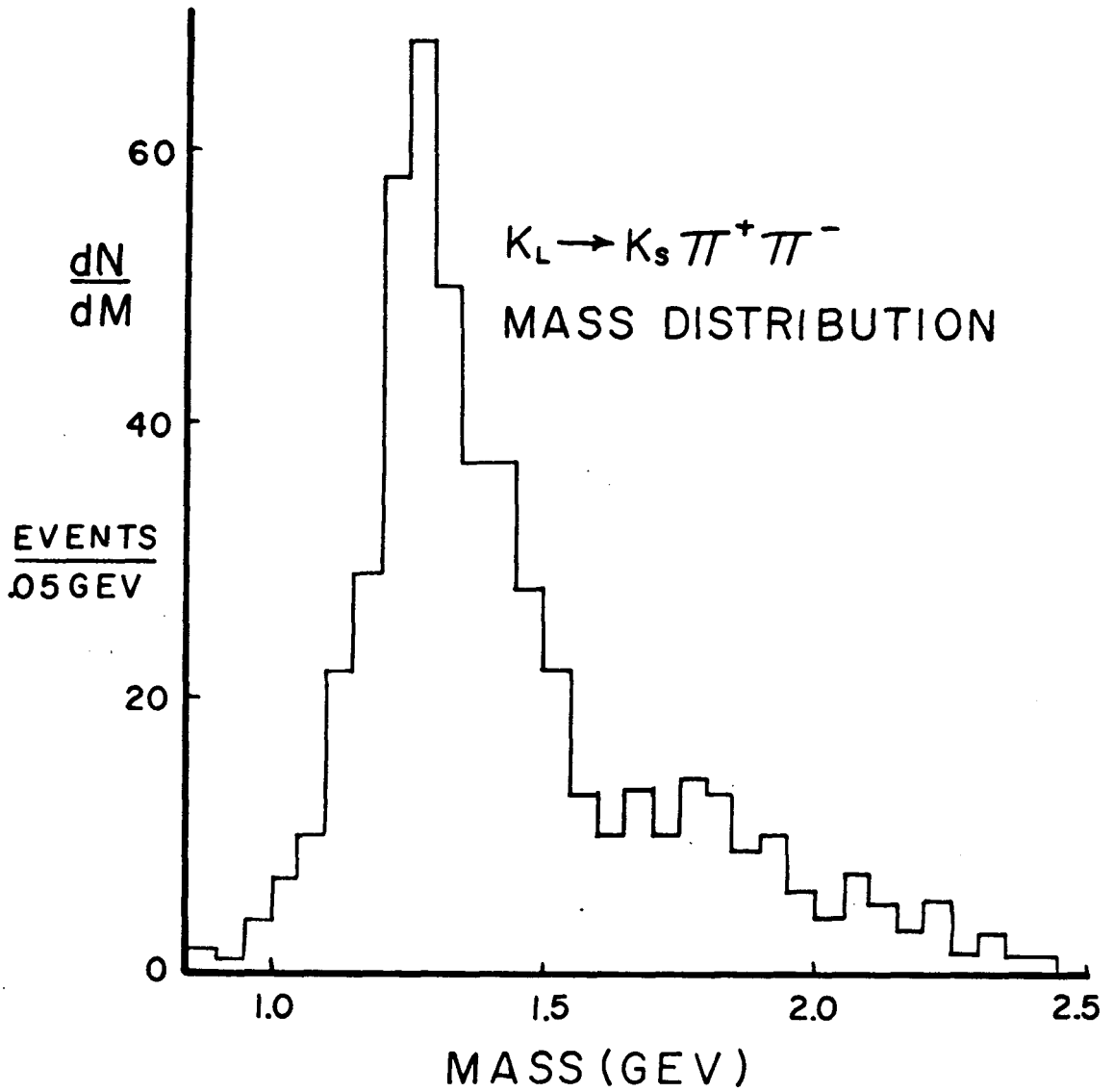

Fig. 15 Mass distribution of $K_o \pi^+ \pi^-$ induced mainly by K_L

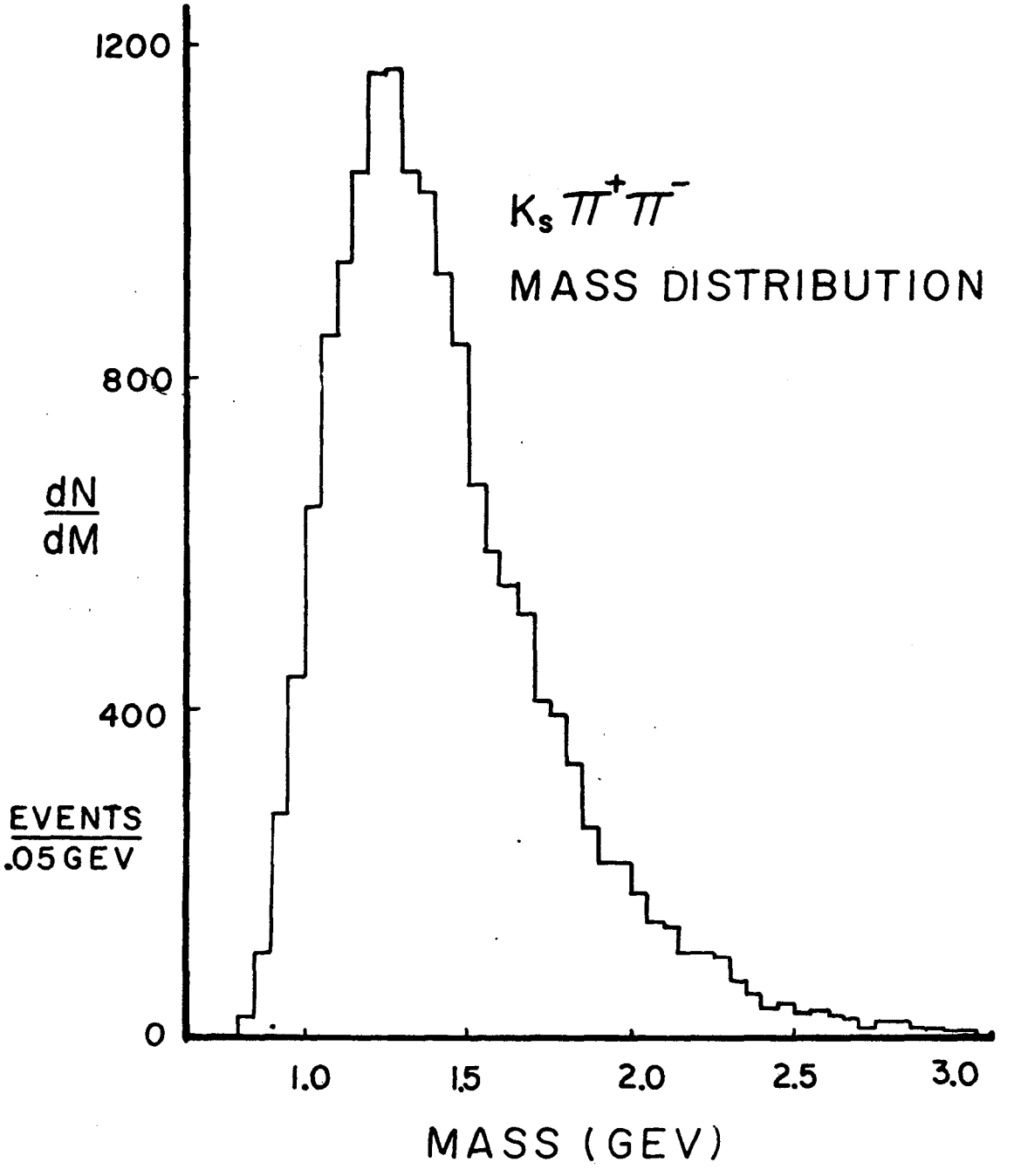

Fig. 16 Mass distribution of $K_o \pi^+ \pi^-$

beam. We observe a clear peak at Q meson mass.

The limit on the production cross section for $M_C \simeq 2$ GeV is

$$\sigma(\gamma + Be \rightarrow C + \bar{C} + \ldots) < 5 \times 10^{-33}\ cm^2/\text{nucleon}.$$
$$\hookrightarrow K_o \pi^{\pm}$$

We would like to remark that the value of the upper limit is smaller than the ψ photoproduction cross section. We have not computed geometric acceptance for other decay modes. Similar limits can be placed on $C \rightarrow \Lambda^o + n\pi$, $\bar{C} \rightarrow \overline{\Lambda^o} + n\pi$ for $1 < n < 4$.

We have also studied the reaction

$$\gamma + Be \rightarrow V + Be$$
$$\hookrightarrow \text{hadrons}$$

where V is a diffractively photoproduced hadronic particle.

We select events which have no hits in AW and AB counters. We study two, four and six charged particles and no π^o's in the final states. The mass and momentum transfer are calculated, assuming they are charged pions. The momentum transfer square of the two charged particle final states is shown in Fig. 9. As stated before, we see clearly the diffractive process on Be nucleus. Similar momentum transfer distributions are observed for four and six charged particle final states. In order to enhance the diffractive process, we make a cut at the transverse momentum square $-t < 0.025$ GeV^2. The mass distributions for two, four, and six charged particle final states are shown in Figs. 17, 18 and 19, respectively. The dashed curve is the acceptance of our detector for the phase space final states. The events plotted are corrected for acceptance. We clearly observe $\rho \rightarrow \pi^+\pi^-$ and $\rho' \rightarrow \pi^+\pi^-$ and $\pi^+\pi^-\pi^+\pi^-$. We have not completed the analysis to obtain the energy dependence of ρ and ρ' photoproduction cross sections and to get the branching ratio $\rho' \rightarrow \pi^+\pi^-/\rho' \rightarrow \pi^+\pi^-\pi^+\pi^-$. For the six charged particle final states, we need more events before we can draw any definite conclusions.

I would like to express my thanks to my colleagues on the experiment.

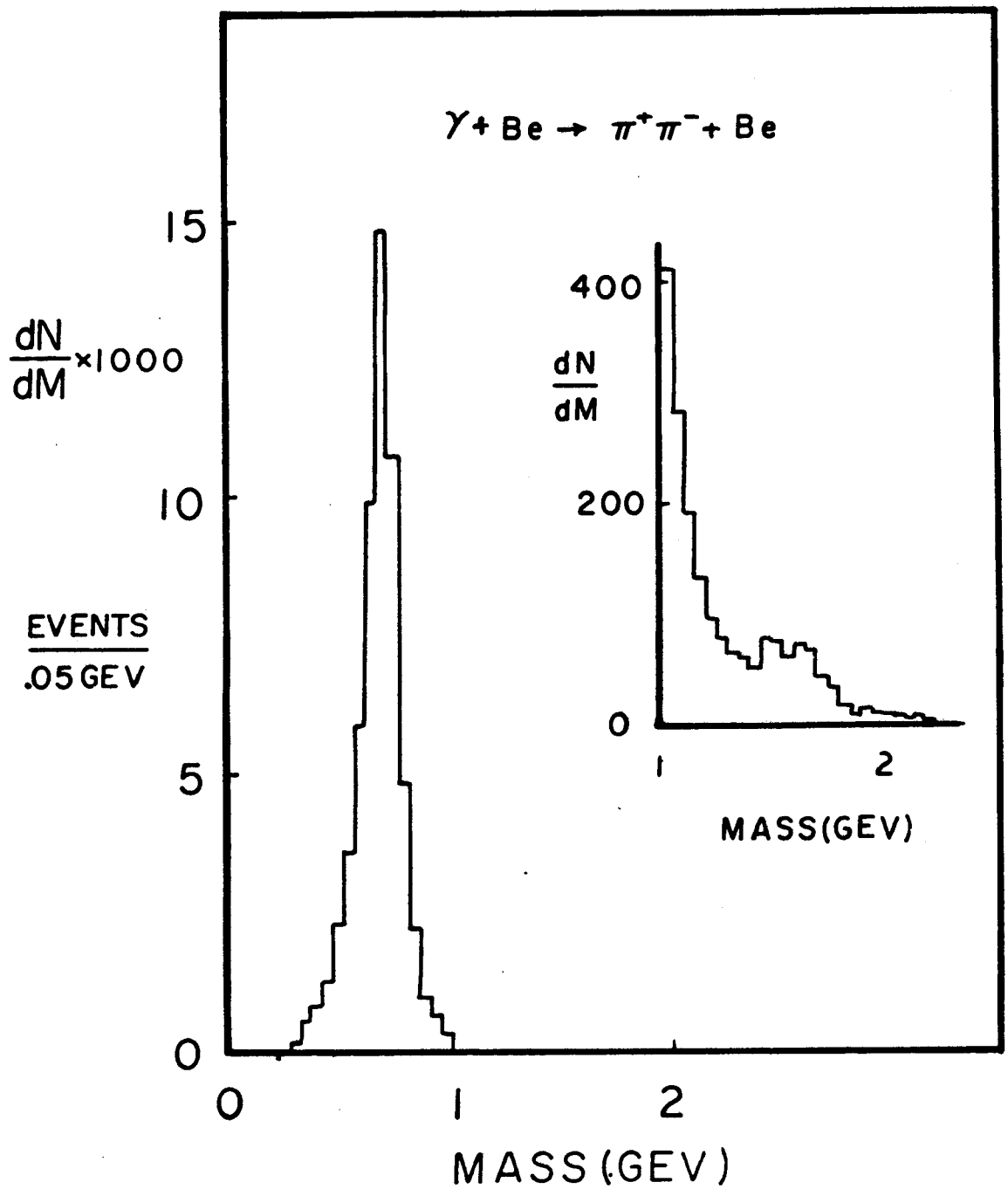

Fig. 17 Mass distribution of two charged particle final states

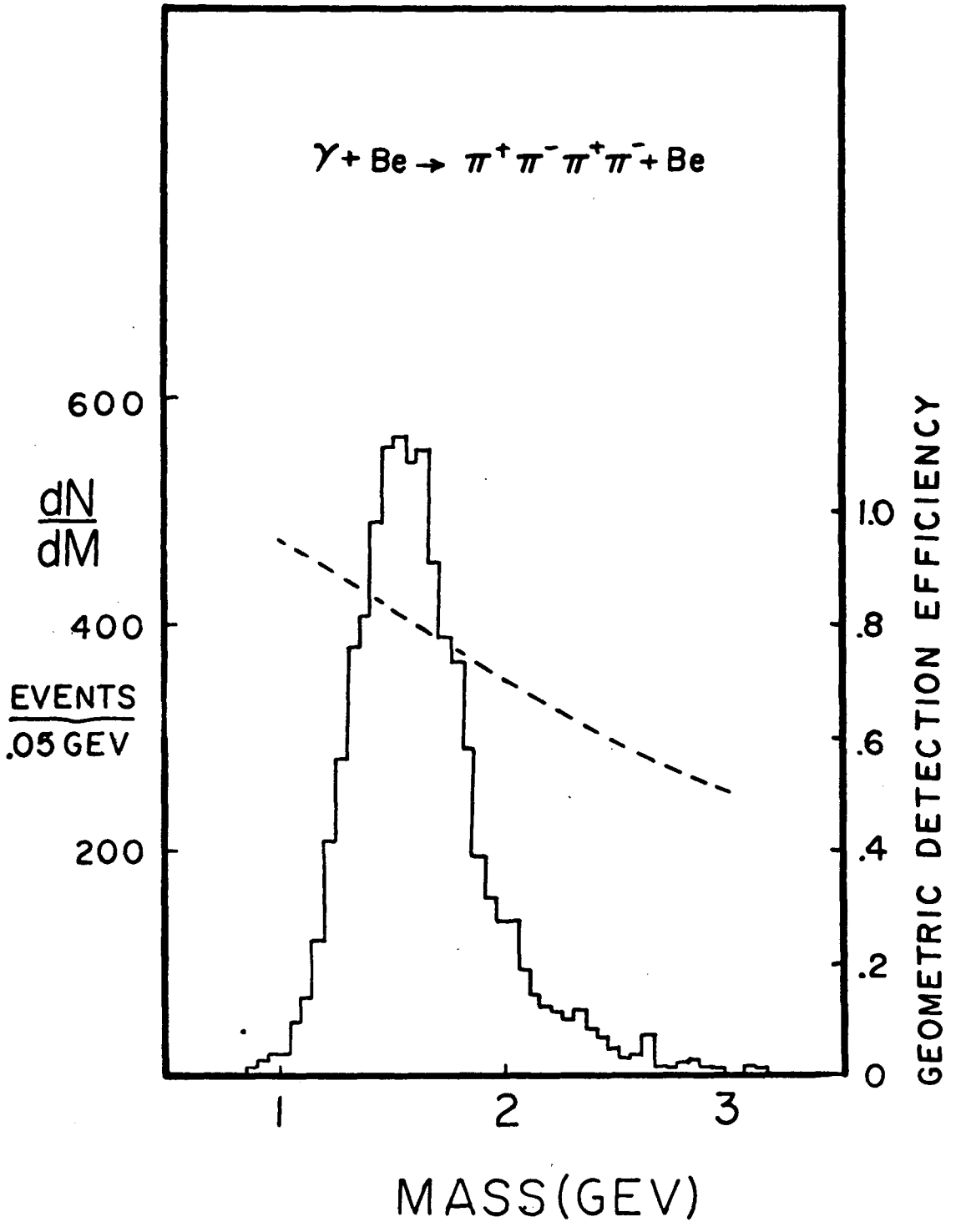

Fig. 18 Mass distribution of four charged particle final states

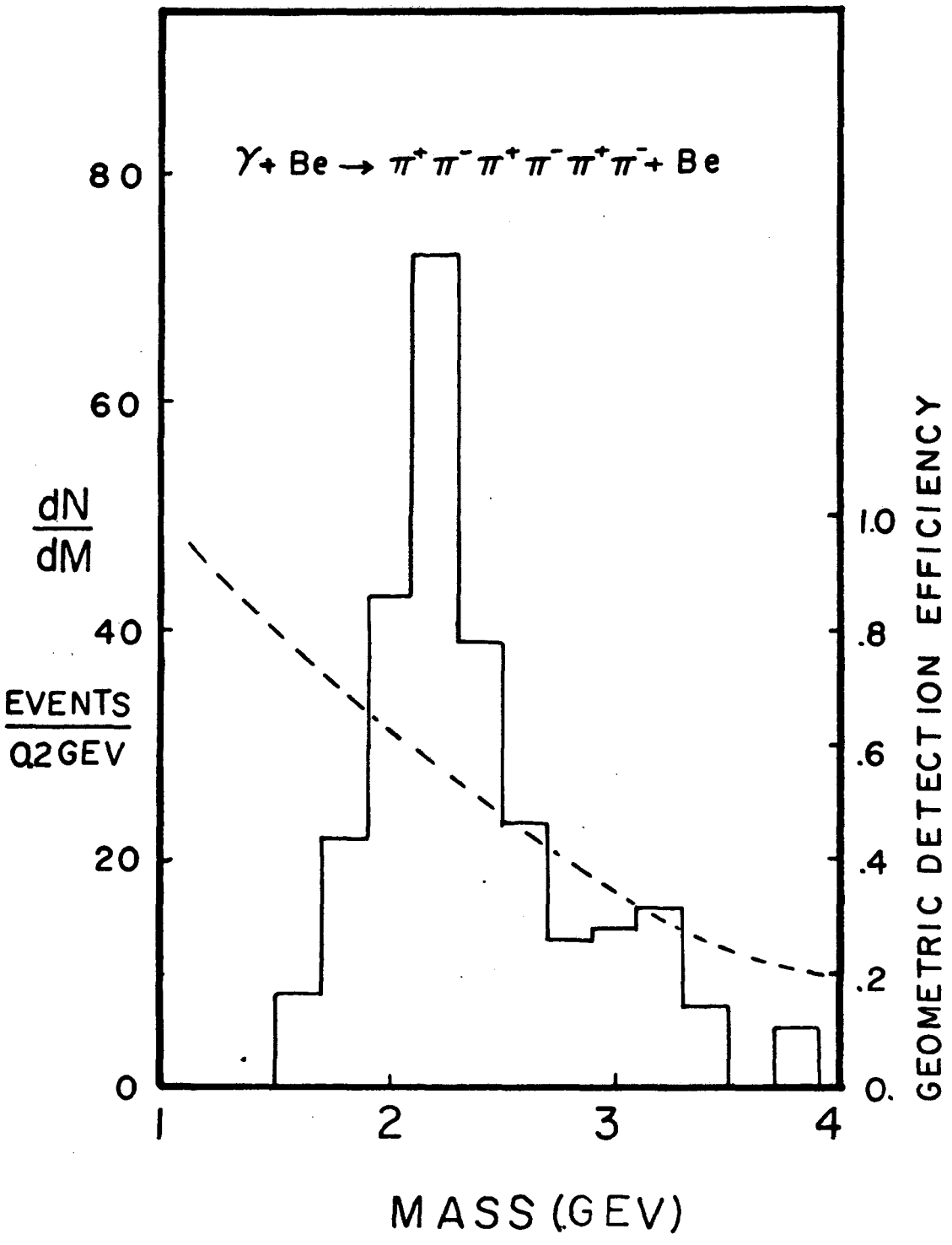

Fig. 19 Mass distribution of six charged particle final states

References

1 J.J. Aubert et al, Phys. Rev. Letters 33, 1404 (1974); J.E. Augustin et al, Phys. Rev. Lett. 33, 1406 (1974). We will call the 3.1 resonance J in hadron collisions and ψ in the photoproduction experiment.

2 B. Knapp, W. Lee, P. Leung, S.D. Smith, A. Wijangco, J. Knauer, D. Yount, D. Nease, J. Bronstein, R. Coleman, L. Cormell, G. Gladding, M. Gormley, R. Messner, T. O'Halloran, J. Sarracino, A. Wattenberg, D. Wheeler, M. Binkley, R. Orr, J. Peoples, L. Read, Phys. Rev. Lett. 34, 1040 (1975); 34, 1044 (1975).

3 T. Nash, Status Report on the 300 GeV Electron Tagged Photon Facility at Fermilab. Paper submitted to the International Symposium on Electron and Photon Interactions at High Energies, Bonn, Germany, August (1973).

4 P. Tsai, Rev. Mod. Phys. 46, 840 (1974).

* Research supported in part by the National Science Foundation.